Mechanism of Atmospheric Photooxidation of Aromatics: A Theoretical Study

Jean M. Andino,[†] James N. Smith,[‡] Richard C. Flagan,[†] William A. Goddard, III,[§] and John H. Seinfeld*,[†]

Departments of Chemical Engineering, Environmental Engineering Science, and Chemistry, California Institute of Technology, Pasadena, California 91125

Received: October 3, 1995; In Final Form: December 13, 1995[⊗]

The mechanisms of atmospheric photooxidation of aromatic compounds are of seminal importance in the chemistry of the urban and regional atmosphere. It has been difficult to experimentally account for the full spectrum of oxidation products in laboratory studies. In an effort to fully elucidate the atmospheric reaction pathways for the aromatic−OH reaction, we have conducted theoretical calculations on aromatic intermediates. Energies have been determined for these intermediates by using semiempirical UHF/PM3 geometry optimizations combined with *ab initio* calculations using density functional theory (DFT). A hybrid DFT model, the Becke3 parameter function with the nonlocal correlation function of Lee, Yang, and Parr, was used in conjunction with the 6-31G(*d*,*p*) basis set to study the intermediate structures. Full mechanisms for the OH-initiated photooxidation of toluene, *m*-xylene, *p*-xylene, 1,2,4-trimethylbenzene, and *m*-ethyltoluene are developed. The lowest energy intermediates have been determined, and predicted products from these structures are compared to available experimental product data. These studies serve to refine proposed mechanisms currently available for toluene, *m*-xylene, and *p*-xylene, while providing new information on the 1,2,4-trimethylbenzene and *m*-ethyltoluene reaction pathways.

1. Introduction

Aromatic compounds are of great interest in atmospheric chemistry because of their abundance in motor vehicle emissions and because of their reactivity with respect to ozone and organic aerosol formation. An understanding of the atmospheric oxidation mechanisms of aromatics has long been cited as the most critical need for further development of reaction mechanisms for the urban and regional atmosphere.[1] The major atmospheric sink for aromatics is reaction with the hydroxyl radical. Whereas rate constants for the OH reaction with aromatics have been well characterized,[2] mechanisms of aromatic oxidation following the initial OH attack have been highly uncertain. In experimental photooxidation studies of toluene, *m*-xylene, and *p*-xylene (summaries of which are available in refs 2−4), typically less than 50% of the reacted carbon has been identified as products. The difficulty in accounting for the remaining fraction of reacted carbon lies in the fact that the intermediates involved in aromatic−OH oxidation have not been unambiguously identified. Consequently, theoretical studies can be extremely useful in evaluating the possible mechanisms of oxidation. We present here theoretical calculations on possible structural intermediates formed in the OH-initiated reactions of toluene, *m*-xylene, *p*-xylene, 1,2,4-trimethylbenzene, and *m*-ethyltoluene. The aromatics chosen correspond to ones that our group has studied in the laboratory. From these energy determinations, the most likely intermediate species have been identified, and overall mechanisms for the photooxidation of these aromatics are proposed.

The aromatic−OH reaction proceeds by both abstraction and addition pathways (see refs 2 and 3 and references cited therein). The addition pathway, occurring roughly 90% of the time, is the more prevalent route. Products identified in the OH addition reactions of toluene, *m*-xylene, and *p*-xylene in previous laboratory studies appear in Tables 1−3. The yields presented in the tables are defined as the ratio of the molar concentration of the product to that of the reacted aromatic. As noted earlier, generally less than 50% of the carbon in these systems has been accounted for experimentally. In the current study, we compare available experimental product data for the toluene, *p*-xylene, and *m*-xylene systems to our proposed mechanisms to evaluate the extent of agreement between the theoretical mechanisms and observed product data. The theory is then used to predict additional products that might be found in these three systems. Since only two studies on products resulting from 1,2,4-trimethylbenzene photooxidation are available,[5,6] neither considering the full mechanism for photooxidation, and no product data on the reactions of *m*-ethyltoluene are available, we develop

TABLE 1: Toluene Photooxidation Products: Molar Yields

compound	yield	ref
glyoxal	0.105 ± 0.019	6
	0.058	7
	0.150 ± 0.040	8
	0.080	9
methylglyoxal	0.146 ± 0.006	6
	0.077	7
	0.140 ± 0.04	8
	0.075	9
methylbutenedial	0.058	7
hydroxymethylbutenedial	0.034	7
oxoheptadienal	0.027	7
methyl hydroperoxide	0.018	7
formaldehyde	0.010	7
hexadienyl	0.010	7
hydroxyoxoheptadienal	0.010	7
maleic anhydride	0.040 ± 0.004	8
o-cresol	0.204 ± 0.027	10
m- and *p*-cresol	0.048 ± 0.009	10
m-nitrotoluene	$(0.0135 \pm 0.0029) + (1.90 \pm 0.25)10^{-16}[NO_2]$	10
o-nitrotoluene	0.07[*m*-nitrotoluene]	10
p-nitrotoluene	0.35[*m*-nitrotoluene]	10

* Author to whom correspondence should be directed.
[†] Department of Chemical Engineering.
[‡] Department of Environmental Engineering Science.
[§] Department of Chemistry.
[⊗] Abstract published in *Advance ACS Abstracts,* June 1, 1996.

S0022-3654(95)02935-2 CCC: $12.00

TABLE 2: *m*-Xylene Photooxidation Products: Molar Yields

compound	yield	ref
glyoxal	0.13 ± 0.03	11
	0.086	12
	0.086 ± 0.011	6
methylglyoxal	0.42 ± 0.05	11
	0.375	12
	0.319 ± 0.009	6
formaldehyde	0.17 ± 0.02	11
2,4-dimethylphenol	0.099	13
2,6-dimethylphenol	0.111	13
4-nitro-*m*-xylene	0.0018	13
5-nitro-*m*-xylene	$0.0032 + 1.6 \times 10^{-17}[NO_2]$	13

TABLE 3: *p*-Xylene Photooxidation Products: Molar Yields

compound	yield	ref
glyoxal	0.24 ± 0.02	11
	0.225 ± 0.039	6
methylglyoxal	0.12 ± 0.02	11
	0.105 ± 0.034	6
3-hexene-2,5-dione	detected	11
formaldehyde	0.17 ± 0.02	11
2,5-dimethylphenol	0.188	13
2-nitro-*p*-xylene	$0.0120 + 2.8 \times 10^{-17}[NO_2])$	13

plausible atmospheric reaction mechanisms for both of these species on the basis of theory alone.

2. Calculation Methods

The essential element of the theoretical approach is to employ semiempirical and *ab initio* quantum mechanical techniques to determine the most energetically favored intermediates in the reaction mechanisms, taking into account transition state complexes. These methods are used to determine the lowest energy structures in the most computationally efficient manner, balancing the desire for reasonable computational times with the highest level of theory. Semiempirical optimizations require less computational time, and given that all of the structures studied are similar in nature (aromatic structures with C, N, O, and H atoms), semiempirical optimizations are adequate for screening and optimizing the structures, while *ab initio* calculations provide accurate energy determinations.

To examine the effectiveness of semiempirical optimizations followed by *ab initio* calculations, studies were conducted on a variety of compounds, including methylhydroxycyclohexadienyl radicals resulting from toluene photooxidation, alkyl radicals, alkoxy radicals, and nitroalkenes, by using different geometry optimization and single-point energy calculation schemes. The first study compared the use of high- and low-level computational techniques to examine methylhydroxycyclohexadienyl radical formation from OH addition to toluene. Since experimental data for the energies of these radicals are not available, comparisons of theoretical and experimental results are not possible. However, these calculations were used to find a balance between the highest level of theory and the computational time required to accurately predict the stability of radicals that are similar to those studied in this work, assuming that the most rigorous computational method adequately reflects the true energy of the species. The second study compared the results of the chosen computational technique to experimental values to provide a calibration of the technique.

Techniques used for geometry optimization include density functional theory (DFT)[14] using the hybrid density function, Becke3LYP, of Becke[15,16] and Lee *et al.*[17,18] and a 6-31G(*d*,*p*) basis set, restricted open-shell Hartree−Fock (ROHF) optimization using a 6-31G(*d*,*p*) basis set, a semiempirical unrestricted Hartree−Fock PM3 (UHF/PM3) optimization,[19] and a molecular mechanics optimization using the MM+ functional form.[20] Of the semiempirical techniques, the PM3 parametrization, a modified neglect of diatomic overlap (MNDO) method, is most often cited as producing the best optimizations for hydrocarbon systems and complexes containing nitrogen and oxygen.[19,21] In addition to providing an accurate geometry, PM3 has also been shown to provide accurate vibrational frequencies that can be directly compared to experiment without *post hoc* correction.[22] These vibrational frequencies allow for the calculation of zero-point energies. The MM+ functional form of the potential was used in the molecular mechanics optimizations since it is most appropriate for small organic molecules.[20]

TABLE 4: Relative Energies (in kcal/mol) for Isomers of the Methylhydroxycyclohexadienyl Radical Using Various Computational Methods[a]

geometry opt/single-point calculation methods	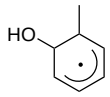	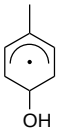	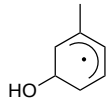
Becke3LYP/Becke3LYP	0[b]	1.1	1.8
ROHF/Becke3LYP	0[c]	0.9	1.7
ROHF/ROHF	0[d]	0.8	0.7
UHF-PM3/Becke3LYP	0[e]	1.2	1.6
MM/Becke3LYP	0.1	0[f]	0.4

[a] The 6-31G(*d*,*p*) basis set was used for all *ab initio* calculations. Footnotes *b*−*f* are absolute energies. [b] −347.3406 au. [c] −347.3364 au. [d] −345.1331 au. [e] −347.3374 au. [f] −347.3318 au.

The DFT and ROHF optimizations were performed on HP 9000/735 workstations using Gaussian 92[18] and PSGVB version 2.13,[23] respectively, while the UHF/PM3 and molecular mechanics optimizations were performed on a personal computer using Hyperchem release 4.0.[24] Single-point calculations were performed by following geometry optimizations utilizing either the ROHF method or density functional theory[14] using the Becke3LYP hybrid density function. Both types of calculations employed a 6-31G(*d*,*p*) basis set and were performed on NP 9000/735 workstations using Gaussian 92.[18] The results for the methyhydroxycyclohexadienyl radicals are given in Table 4, with relative energy defined as the difference in energy between any given structural isomer and the lowest energy structural isomer. Table 4 indicates that the MM+ optimization, followed by the DFT calculation, does not reproduce the results of the high-level DFT optimization followed by the DFT calculation. The UHF/PM3 geometry optimization method, however, gives relative energies that are quite close to the DFT values. Of the techniques studied, a semiempirical UHF/PM3 geometry optimization, followed by a single-point calculation using the Becke3LYP density function and a 6-31G(*d*,*p*) basis set, exhibits the best combination of computational efficiency and accuracy. This method therefore was chosen for all of the calculations that are presented in this study.

To calibrate the chosen computational scheme, a second study was performed. Geometry optimizations using the UHF/PM3 method followed by a single-point calculation using the Becke3LYP density function and a 6-31G(*d*,*p*) basis set were performed on radicals and stable species for which experimental energy data exist. The relative energies of isomers of the structures were compared and are tabulated in Table 5. From this table it is evident that the PM3/Becke3LYP technique adequately reproduces the relative energies between structural isomers for several different classes of compounds. In addition, we can obtain an estimate of our accuracy by comparing experimentally derived and theoretical relative energies. These values differ by at most 1.6 kcal/mol (which can be rounded to

TABLE 5: Comparison of Relative Energies of Different Structural Isomers Based on Experimental Data and Theoretical Calculations

structure	relative energy, experiment[a] (kcal/mol)	relative energy, calculated[b] (kcal/mol)
	3.8	4.3
	0	0
	4.9	3.3
	0	0
	6.6	6.1
	0	0
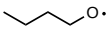	2.6	3.3
	0	0
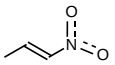	5	5.1
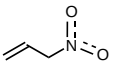	0	0

[a] Experimental data from NIST Standard Reference Database 25.[28] [b] Relative energies determined by using UHF/PM3 geometry optimization followed by Becke3LYP single-point energy calculation.

TABLE 6: Comparison of Experimentally and Theoretically Derived ΔH Values for the Toluene + OH Reaction

reactants	products	ΔH_{rxn}, theoretical (kcal/mol)	ΔH_{rxn}, experimental (kcal/mol)
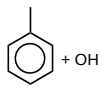	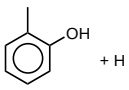	+1.38	+0.8 ± 0.4
	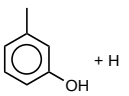	+1.25	−0.8 ± 0.7
	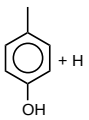	+1.94	+0.9 ± 0.4

2 kcal/mol). As a further calibration, ΔH_{rxn} values derived from literature data[25] and PM3/DFT calculations for the toluene + OH reaction, resulting in the formation of cresol isomers, are compared. These data appear in Table 6 and show agreement between experiment and theory to within 2 kcal/mol. Although the ΔH_{rxn} comparisons between experiment and theory are within 2 kcal/mol agreement for the case presented in Table 6, it is difficult to say that the agreement between experiment and theory will be at the level of 2 kcal/mol for all cases studied in this work. However, because literature data were not available to indicate a reasonable level of error for ΔH_{rxn} values, and because we have not performed a variety of ΔH_{rxn} calculations on reactions involving the alteration of carbon centers, interpretations of inclusions/exclusions of reaction pathways are limited to those that involve large differences between ΔH_{rxn} values for different reaction pathways.

Because molecular mechanics provides a fast first approximation to the optimized structure, this technique was used before employing the UHF/PM3 method in the present study of aromatic mechanisms. To examine whether the individual structures investigated were at global rather than local minima, several starting geometries of each structure were subjected to geometry optimization calculations. The heats of formation (obtained at the PM3 level) of the different geometries were compared, and the lowest energy structure was chosen for subsequent single-point *ab initio* calculations. In cases where the semiempirically derived heats of formation were similar, several conformations were subjected to single-point *ab initio* calculations to locate the lowest energy conformation. All structures were characterized as being genuine minima (i.e., having no imaginary frequencies) at the PM3 level. The Becke3LYP energy was subsequently corrected to 298 K by using the normal mode vibrational frequencies and thermal corrections obtained at the PM3 level. Thus, it is this corrected energy that is used to determine the lowest energy intermediate species in a particular step of the reaction mechanism.

Transition states were calculated with a constrained optimization procedure at the UHF/PM3 level by using Gaussian 92. Conventional direct optimization schemes available through Gaussian 92 were attempted. However, because of the complexity of the structures studied, it was difficult to locate the structure with an initial geometry corresponding to a single negative eigenvalue of the second-derivative matrix, a condition that is necessary before a conventional transition state optimization can proceed. The constrained optimization method relies on the assumption that the transition states are governed by the formation of a single bond in each step (for example, the C−O bond in the formation of the methylhydroxycyclohexadienyl radicals). Thus, the bond distance is adjusted by small increments (0.1 Å steps in this case) and frozen, while the geometry of the molecule is optimized. At the end of each optimization, the PM3-derived energy of the structure is noted. This procedure is repeated until a point of maximum energy is obtained. The constrained optimization procedure at the UHF/PM3 level was used to obtain an initial estimate of the transition state. Once this estimated transition state structure was found, DFT single-point calculations were performed on this structure, and small geometrical perturbations of the structure to ensure that the UHF/PM3-constrained optimization was successful in determining an estimate for the transition state geometry. This estimate of the true transition state is assumed to be an upper limit to the first-order saddle point due to the elementary means of accounting for electron correlation. Because of the large number of structures considered in this study, transition states were located for representative cases and subsequently applied to homologous transition state complexes.

3. Results of Calculations

A generalized summary of the steps considered in the OH−aromatic mechanism appears in Figure 1. Each reaction is subsequently treated individually. Figures 2−6 show the reaction coordinate diagrams (relative energy in kilocalories/mole versus reaction path) for the lowest energy structures found for each of the five aromatic−OH reactions. Energy and geometry data for the various structures studied in this work are available throughout this paper for comparison. Additional data are available from the authors upon request.

3.1. Initial Hydroxyl Radical Attack. There are several possible sites of attack for the OH radical in each of the aromatics considered. Some sites are less sterically hindered than others or are favored because of stabilizations as a result of group interactions. If we consider the transition states leading to the formation of the substituted hydroxycyclohexadienyl radicals, the aromatic−OH adducts formed in reaction 1b, we

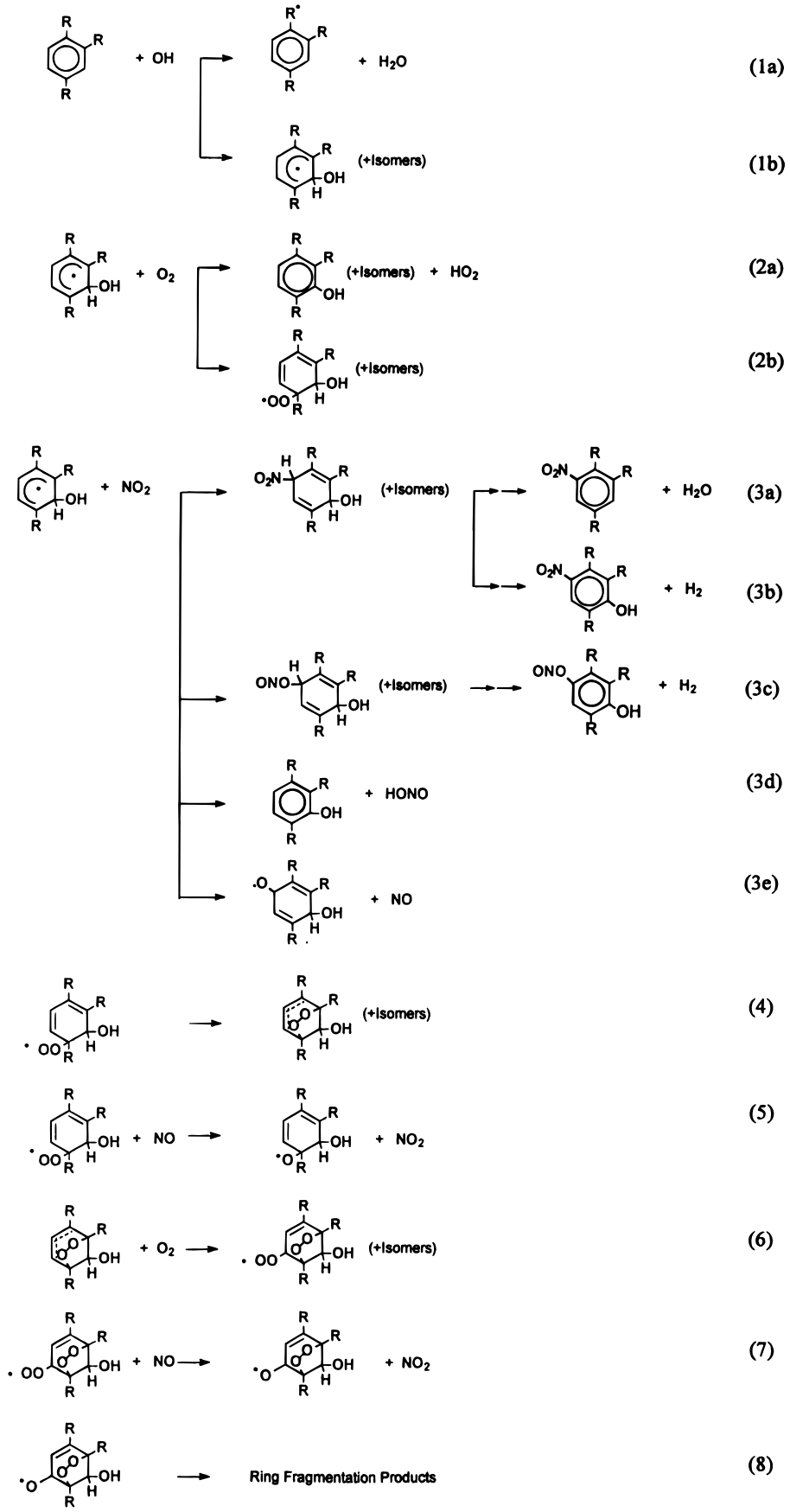

Figure 1. Possible reactions in a generalized mechanism of aromatic−OH photooxidation. R represents either an H atom or an alkyl group, depending on the aromatic considered.

find that the barrier heights are essentially negligible. Several different geometries were considered for each aromatic. Shown in Table 7 are the PM3-derived equilibrium structures for a representative sample of the most stable aromatic−OH adducts. Total energies for aromatic−OH adducts are tabulated in Table 8. Indicated are single-point energies at 0 K derived by using

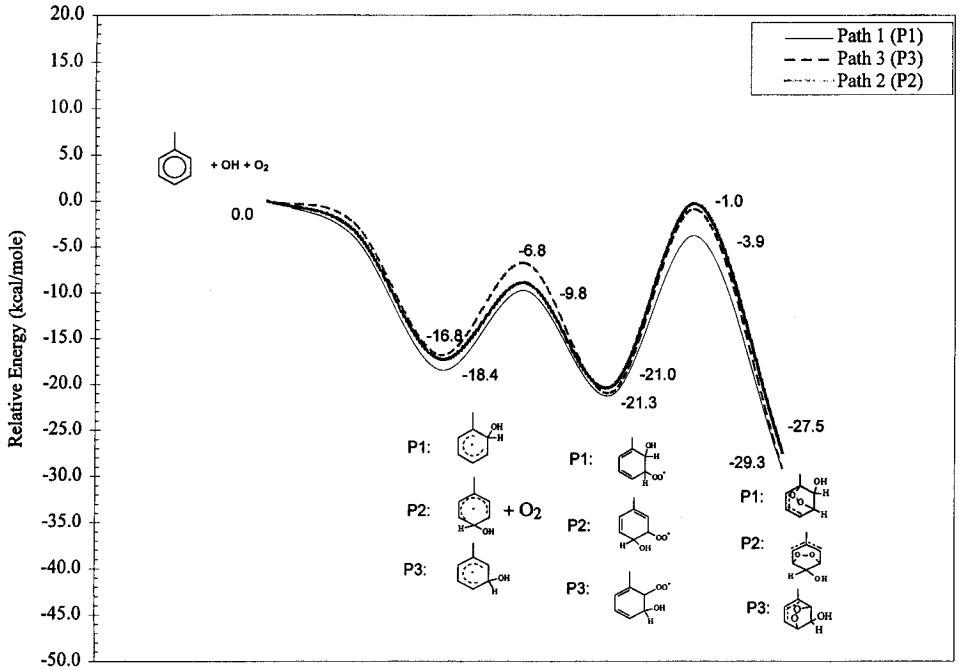

Figure 2. Reaction coordinate diagram for toluene. Indicated are the three favored pathways. Shown below the plots are the corresponding aromatic−OH adduct, peroxy radical, and bicyclic radical corresponding to the pathways. The structures are labeled P1, P2, and P3, corresponding to paths 1, 2, and 3, respectively.

TABLE 7: PM3 Equilibrium Structures for a Representative Selection of the Most Stable Reaction Products of Aromatics with OH (Reaction 1b)[a]

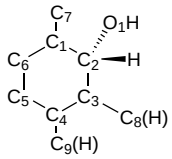

parameter	toluene	*m*-xylene	*p*-xylene	*m*-ethyltoluene
$r(C_1,C_2)$	1.505	1.507	1.505	1.507
$r(C_2,O_1)$	1.414	1.416	1.415	1.416
$r(C_2,C_3)$	1.498	1.507	1.497	1.507
$r(C_3,C_4)$	1.370	1.379	1.377	1.379
$r(C_4,C_5)$	1.411	1.407	1.416	1.408
$r(C_5,C_6)$	1.406	1.407	1.405	1.407
$r(C_6,C_1)$	1.381	1.379	1.381	1.379
$r(C_1,C_7)$	1.479	1.479	1.478	1.479
$r(C_3,C_8)$		1.479		1.490
$r(C_4,C_9)$			1.486	
$\angle(C_1,C_2,C_3,O_1)$	128	127	127	128

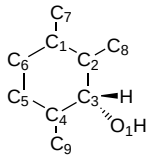

parameter	1,2,4-tmb
$r(C_1,C_2$	1.388
$r(C_3,O_1)$	1.417
$r(C_2,C_3)$	1.507
$r(C_3,C_4)$	1.506
$r(C_4,C_5)$	1.378
$r(C_5,C_6)$	1.406
$r(C_6,C_1)$	1.413
$r(C_1,C_7)$	1.486
$r(C_2,C_8)$	1.480
$r(C_4,C_9)$	1.479
$\angle(C_2,C_3,C_4,O_1)$	127

[a] All bond distances are in angstroms and all angles are in degrees.

density functional theory and energies corrected to 298 K by using vibrational information generated at the PM3 level. In general, the preferred place of OH addition, based on the total energies of the aromatic−OH adducts, is a position ortho to a substituent methyl group. In considering the total energies of each of the aromatic−OH isomers, we did, however, find that there were some cases where isomers had energies within 2 kcal/mol of the lowest energy structures. Therefore, whereas the structures with OH attachment at the ortho position are lowest in energy, pathways that include aromatic−OH structures whose relative energy falls within ±2 kcal/mol of the lowest energy isomer will also be considered. Throughout our discussion, we compare available experimental product data to results predicted by the theoretical calculations. This comparison serves two purposes: to lend credence to our uncertainty limit of 2 kcal/mol and to show that the theoretical predictions are adequate representations of atmospheric and/or experimental conditions.

3.1.1. Toluene. The lowest energy aromatic−OH structure for toluene is that resulting from addition to the ortho position. However, OH additions to the meta and para positions yield structures that are only 1.6 and 1.2 kcal/mol higher in energy than addition at the ortho site. Thus, on the basis of theoretical considerations, additions to the meta and para positions cannot be excluded from reaction mechanism considerations. Following formation of the adduct, molecular oxygen can abstract a hydrogen atom to form a cresol. There is experimental evidence for *o*-, *m*-, and *p*-cresols, with the *o*-cresol yield dominating cresol formation (Table 1), which is consistent with the theoretical predictions.

3.1.2. m-Xylene. The lowest energy aromatic−OH structure for *m*-xylene also corresponds to OH addition to the 2-position. Additions to the 4- and 5-positions are 0.88 and 3.5 kcal/mol higher in energy, respectively, than addition to the 2-position. Additions to the 6- and 4-positions create identical structures. On the basis of these results, the lowest energy adducts for

TABLE 8: Calculated Energies (in hartrees) of Most Stable Reaction Intermediates for the Reaction Pathway Leading to the Formation of the Bicyclic Endoperoxy Radicals

aromatic			OH addition (reaction 1b)			O_2 addition (reaction 2b)			O_2 bridge formation (reaction 4)		
molecule	E_e^0	E^{298}	site	E_e^0	E^{298}	site[a]	E_e^0	E^{298}	sites	E_e^0	E^{298}
toluene	−271.5774	−271.4454	3	−347.3348	−347.1876	2 (4, 6)	−497.6616	−497.5035	2, 4	−497.6750	−497.5168
			4	−347.3355	−347.1883	3 (1)	−497.6606	−497.5025	3, 5	−497.6721	−497.5139
			2	−347.3374	−347.1902	3 (1, 5)	−497.6621	−497.5040	3, 1	−497.6751	−497.5169
m-xylene	−310.8971	−310.7363	4	−386.6589	−386.4826	5 (3, 1)	−536.9828	−536.7963	5, 3	−536.9962	−536.8086
			2	−386.6603	−386.4840	3	−536.9851	−536.7986	3, 1	−537.0008	−536.8132
p-xylene	−310.8969	−310.7359	2	−386.6253	−386.4492	3 (1, 5)	−536.9848	−536.7968	3, 1	−536.9988	−536.8108
1,2,4-trimethyl-benzene	−350.2154	−350.0250	6	−425.9739	−425.7671	1	−576.3036	−576.0861	1, 5	−576.3194	−576.1019
			3	−425.9773	−425.7705	2	−576.3049	−576.0874	2, 4	−576.3210	−576.1035
			5	−425.9774	−425.7706	4 (2)	576.3031	−576.0856	4, 5	−576.3177	−576.1002
m-ethyltoluene	−350.2116	−350.0216	4	−425.9740	−425.7675	5 (3, 1)	−576.2976	−576.0801	5, 3	−576.3077	−576.0902
			6	−425.9742	−425.7677	5 (1, 3)	−576.2996	−576.0821	5, 1	−576.3114	−576.0939
			2	−425.9751	−425.7686	3 (1, 5)	−576.2967	−576.0792	3, 1	−576.3121	−576.0946

[a] Addition sites in parentheses indicate comparable low-energy structures.

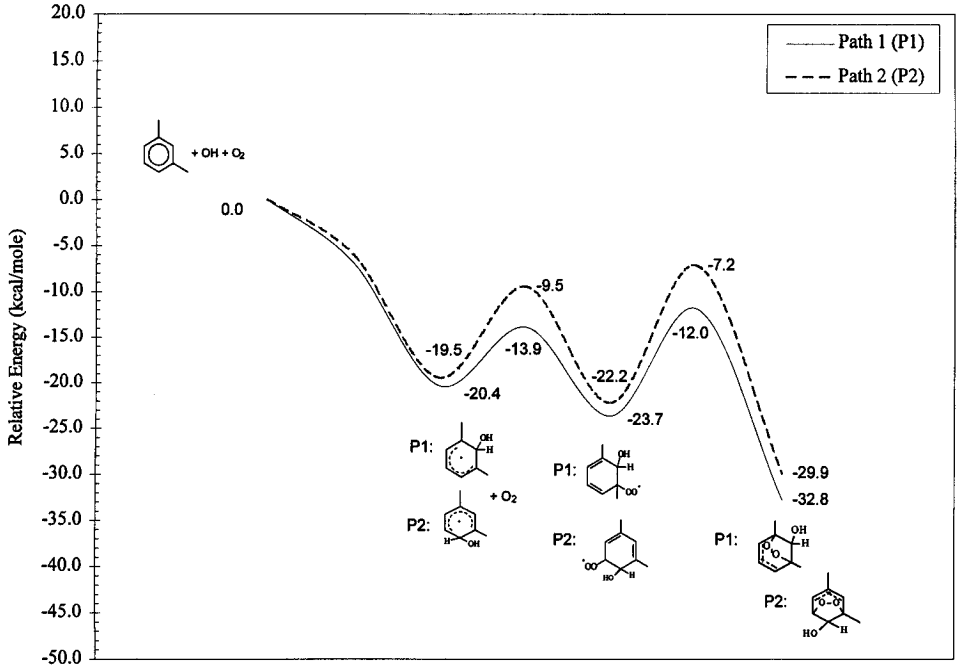

Figure 3. Reaction coordinate diagram for *m*-xylene. Indicated are the energies of the two favored pathways. Shown below the plots are the corresponding aromatic−OH adduct, peroxy radical, and bicyclic radical corresponding to the pathways. The structures are labeled P1 and P2, corresponding to paths 1 and 2, respectively.

m-xylene correspond to OH addition to the 2- and 4-positions, both of which are ortho to one of the substituent methyl groups. The reaction coordinate diagram for *m*-xylene (Figure 3) depicts the lowest energy adducts formed. By comparing the theoretical predictions to experimentally determined products in Table 2, we note experimental evidence for 2,6- and 2,4-dimethylphenol (with the 2,6-dimethylphenol yield dominating), consistent with OH addition to the 2- and 4-positions. There is no experimental evidence for 3,5-dimethylphenol, consistent with our finding that OH addition to the 5-position can be excluded.

3.1.3. p-Xylene. Because of the high degree of symmetry of *p*-xylene, only one structure was considered. The experimental evidence for O_2 reaction with the *p*-xylene−OH adduct, leading to the formation of only 2,5-dimethylphenol (see Table 3), indicates that there is only one possible pathway for OH addition to the ring. The reaction coordinate diagram for *p*-xylene in Figure 4 and Table 7 show the structure for the OH−aromatic adduct.

3.1.4. 1,2,4-Trimethylbenzene. The lowest energy aromatic−OH adducts for trimethylbenzene correspond to OH additions at the 3- and 5-positions. The energies of these two adducts are identical. Addition to the 6-position is 2.1 kcal/mol higher in energy than the other two adducts. The reaction coordinate diagram for 1,2,4-trimethylbenzene in Figure 5 details the path of the favored OH−aromatic adducts structures. Given that there are no experimental data available on the ring-retaining products of 1,2,4-trimethylbenzene, the given energy calculations can be used to predict the phenolic compounds formed. Thus, we predict the formation of 2,3,6-trimethylphenol, 2,3,5-trimethylphenol, and 2,4,5-trimethylphenol from the O_2 reaction with the adducts formed from OH addition to the 3-, 6-, and 5-positions, respectively (according to reaction 2a).

3.1.5. m-Ethyltoluene. The lowest energy aromatic−OH adduct for *m*-ethyltoluene corresponds to OH addition to the 2-position. The energies for the adducts formed from addition to the 4-, 5-, and 6-positions are 0.69, 3.0, and 0.56 kcal/mol higher, respectively, than that for addition to the 2-position. From these values, we conclude that the aromatic−OH adducts to be included in the reaction mechanism for *m*-ethyltoluene include the addition of OH to the 2-, 4-, and 6-positions. Note that these results are very similar to those of *m*-xylene; addition of OH to the 5-position is the least favored radical. Substituent methyl groups have a considerable effect on the favored addition sites for OH. Figure 6 details the paths of the three lowest

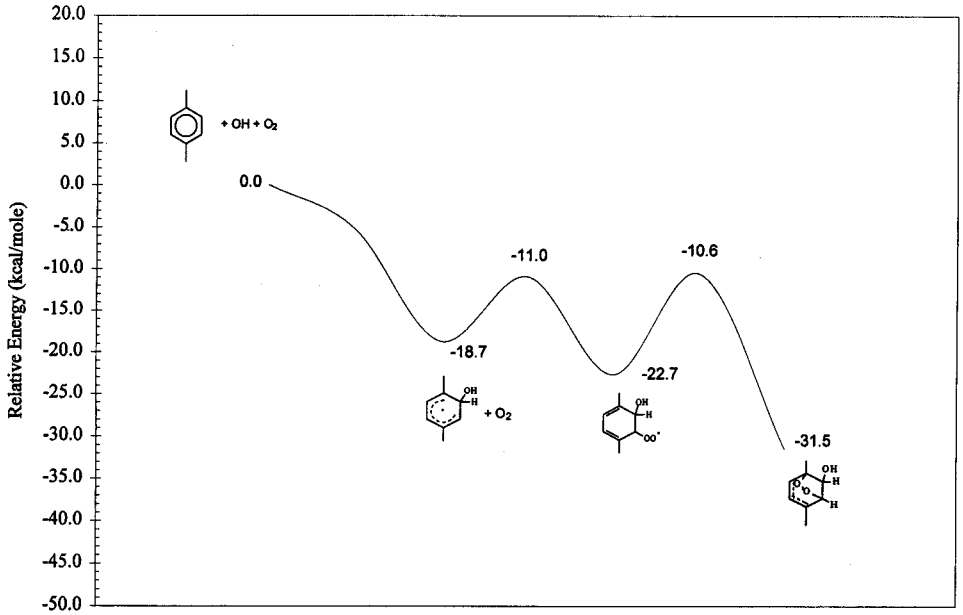

Figure 4. Reaction coordinate diagram for *p*-xylene. Shown below the path are the corresponding aromatic−OH adduct, peroxy radical, and bicyclic radical corresponding to the favored pathway.

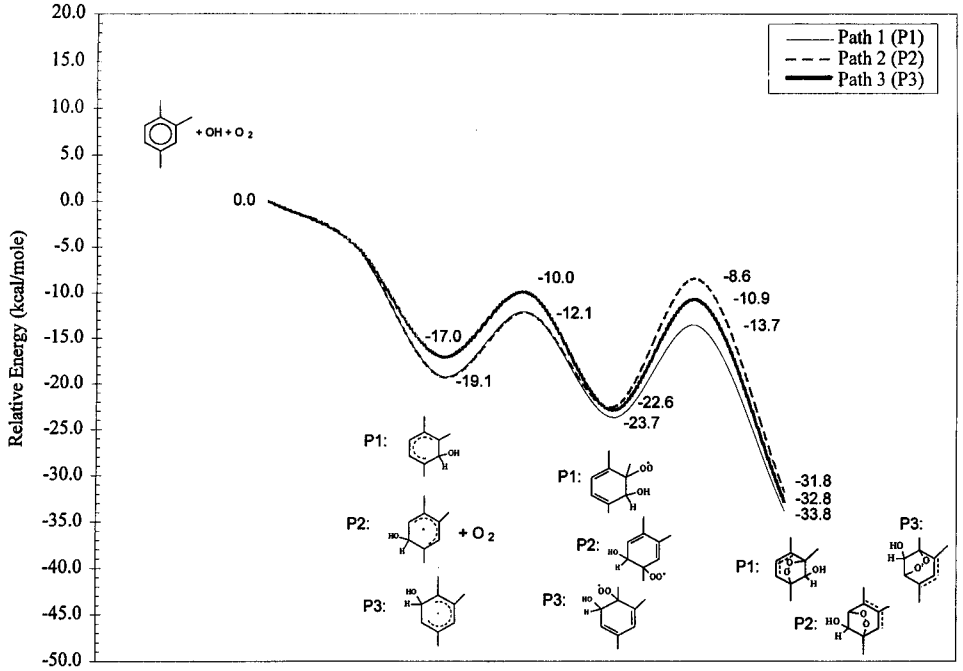

Figure 5. Reaction coordinate diagram for 1,2,4-trimethylbenzene. Indicated are the energies of the three favored pathways. Shown below the diagram are the corresponding aromatic−OH adduct, peroxy radical, and bicyclic radical corresponding to the pathways. The structures are labeled P1, P2, and P3, corresponding to paths 1, 2, and 3, respectively.

energy aromatic−OH structures. As with the case of 1,2,4-trimethylbenzene, there are no experimental data available for ring-retaining products formed from the *m*-ethyltoluene−OH reaction. On the basis of our energy determinations, we predict the formation of 2-ethyl-6-methylphenol, 2-ethyl-4-methylphenol, and 4-ethyl-6-methylphenol from the O_2 reaction with the adducts formed from OH addition to the 2-, 4-, and 6-positions, respectively.

3.2. Fate of the OH−Aromatic Adduct: NO_2 Reaction. It has been suggested that aromatic−OH adducts react with NO_2 to yield nitroaromatics according to reaction 3a of the generalized mechanism.[29] To explain the observed variation in aromatic photooxidation product yields with varying NO_2 concentration, alternative paths for aromatic−OH adduct reaction with NO_2, which results in the formation of oxy type radicals (reaction 3e)[27] or a phenolic type compound and HONO (reaction 3d),[27] have been proposed. Two additional pathways can be suggested for reaction 3: pathway 3c, forming the hydroxyaromatic nitrite, and 3b, forming the hydroxy nitroaromatic (nitrophenol, nitrodimethylphenol, etc.).

Experimental evidence has been found for the presence of nitroaromatic compounds in the photooxidation of toluene, *m*-xylene, and *p*-xylene (see Tables 1−3). While calculations were not performed on all of the nitroaromatic compounds, it will be shown in the discussion that follows that ΔH_{rxn} for reaction 3a is −26.3 kcal/mol for the case of toluene. Thus, the reaction of NO_2 with the OH−aromatic adduct is assumed to be exothermic for all aromatics in this study. The nitroaromatics that are predicted to form involve the reaction of NO_2 with the most stable OH−aromatic adducts, using the conven-

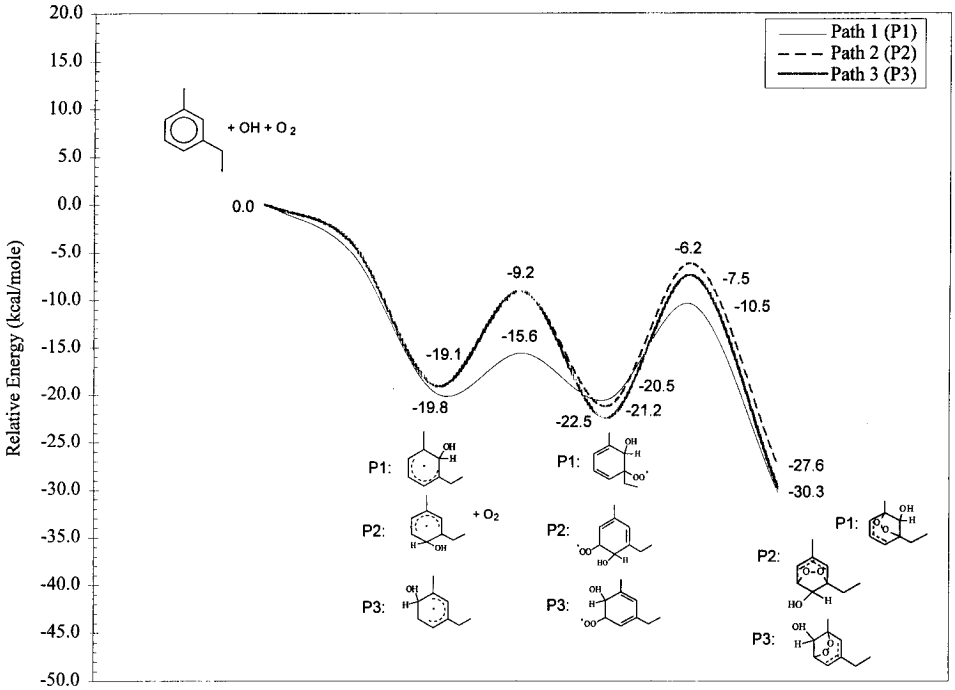

Figure 6. Reaction coordinate diagram for *m*-ethyltoluene. Indicated are the energies of the three favored pathways. Shown in the diagram are the corresponding aromatic−OH adduct, peroxy radical, and bicyclic radical corresponding to the pathways. The structures are labeled P1, P2, and P3, corresponding to paths 1, 2, and 3, respectively.

tional wisdom that NO_2 addition to an alkylhydroxycyclohexadienyl radical will be at a site ortho to the hydroxyl substituent group.[29] Consistent with the theoretical prediction that all three possible toluene−OH adducts form, experimental evidence exists for three different nitrotoluene products. Similarly, consistent with the prediction that only two of the possible *m*-xylene−OH adducts form, experimental evidence exists for only two nitro-*m*-xylene products. Hydroxyl radical addition to the 2-position of *m*-xylene, with subsequent reaction with NO_2, yields 4-nitro-*m*-xylene, whereas addition to the 4-position yields 5-nitro-*m*-xylene. Observations of the nitroaromatics from the *p*-xylene photooxidation systems are also consistent with theory. Only one nitroaromatic, 2-nitro-*p*-xylene, is detected in laboratory studies. Since experimental data are not available for the nitroaromatics resulting from the 1,2,4-trimethylbenzene and *m*-ethyltoluene systems, the results of the previous section, indicating the favored aromatic−OH adducts, can predict the nitroaromatic species expected to form in photooxidation studies of 1,2,4-trimethylbenzene and *m*-ethyltoluene. From OH addition to the 3- and 5-positions, 4-nitro-1,2,4-trimethylbenzene and 6-nitro-1,2,4-trimethylbenzene are predicted to form and 5-nitro-1,2,4-trimethylbenzene should not form. For *m*-ethyltoluene, the formation of 4-nitro-*m*-ethyltoluene from OH addition to the 2-position, 5-nitro-*m*-ethyltoluene from OH addition to the 4-position, and 2-nitro-*m*-ethyltoluene from addition to the 6-position is predicted.

To examine the stabilities of the five competing pathways for aromatic−OH adduct reaction with NO_2, theoretical calculations were performed for the case of toluene. Energies were calculated for nitrotoluene (reaction 3a), nitrophenol (reaction 3b), phenol nitrite (reaction 3c), phenol (reaction 3d), and oxy radicals (reaction 3e). Only one structural isomer for each reaction (3a−3d) was considered. Transition states were determined for the first steps of reactions 3a−3c and for reactions 3d and 3e. Geometrical information for these reaction intermediates as well as for the transition states appears in Table 9. The second steps of reactions 3a−3c were not subjected to transition state analyses since these reactions involve processes (rearrangement and the subsequent loss of water or molecular hydrogen) that are difficult to analyze by using the constrained optimization procedure and are subject to interpretation. Clearly, much additional work is required to completely elucidate the transition states of the second steps of reactions 3a−3c. Even though transition states are not included for the second steps of reactions 3a−3c, valuable information can be gained regarding the relative stability of intermediates, as well as the overall heats of reaction for the reactions considered.

The compounds NO, NO_2, H_2O, and HONO were subjected to the same type of calculations as each of the intermediate species. A PM3 geometry optimization was conducted followed by a Becke3LYP single-point calculation. The single-point energy was subsequently corrected to 298 K by using the normal mode vibrational frequencies and thermal corrections obtained at the PM3 level. Table 10 shows the uncorrected energy at 0 K (from the Becke3LYP single-point calculation) and the corrected energy at 298 K for NO, NO_2, H_2O, HONO, and each of the other species participating in a reaction with an aromatic intermediate. Table 11 contains the energies (0 and 298 K) of all of the products formed in the aromatic−OH adduct reaction with NO_2.

For the case of toluene, as an example, the ΔH_{rxn} for the first steps of pathways 3a−3c and for overall pathways 3d and 3e are −26.3, −26.3, −24.5, −52.8, and +38.3 kcal/mol, respectively. The barrier heights for pathways 3a and 3b (first step), 3c (first step), and 3d are 5, 1, and 2 kcal/mol, respectively. Note that reactions 3c and 3e are assumed to have the same transition state. On the basis of this information for the initial steps of reactions 3a−3c and the overall reactions 3d and 3e, the only pathway that can be unambiguously excluded is reaction 3e because of its endothermic nature. In the absence of additional transition state data regarding the second steps of reactions 3a−3c, it is impossible to recommend the exclusion of one of these pathways. Therefore, until additional data can be obtained for reactions 3a−3c, we recommend the inclusion of reactions 3a−3d in overall mechanisms for aromatic−OH photooxidation. As mentioned previously, it is clear that

TABLE 9: PM3 Geometries for Equilibrium and Approximate Transition State Structures for Reactions of Aromatic−OH Adducts with NO_2[c]

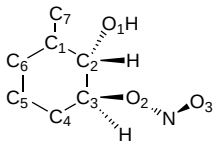

parameter	opt value[a]	TS value[b]
$r(C_1,C_2)$	1.512	
$r(C_2,O_1)$	1.408	
$r(C_2,C_3)$	1.560	
$r(C_3,O_2)$	1.436	2.2
$r(C_3,C_4)$	1.500	
$r(O_2,N)$	1.411	
$r(N,O_3)$	1.164	
$\angle(C_3,O_2,N)$	113	
$\angle(O_2,N,O_3)$	108	
$\angle(C_1,C_2,C_3,O_1)$	127	
$\angle(C_2,C_3,C_4,O_2)$	119	100

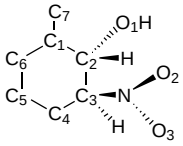

parameter	opt value	TS value
$r(C_1,C_2)$	1.509	
$r(C_2,O_1)$	1.407	
$r(C_2,C_3)$	1.556	
$r(C_3,N)$	1.549	2.6
$r(C_3,C_4)$	1.492	
$r(N,O_2)$	1.211	
$r(N,O_3)$	1.213	
$\angle(C_3,N,O_2)$	120	
$\angle(O_2,N,O_3)$	123	
$\angle(C_1,C_2,C_3,O_1)$	127	
$\angle(C_2,C_3,C_4,N)$	124	101

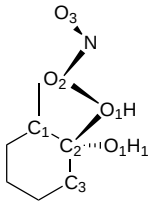

parameter	TS value
$r(C_2,H_2)$	1.0
$r(H_2,O_2)$	1.7
$\angle(C_1,C_2,C_3,H_2)$	37
$\angle(H_2,O_2,N)$	104

[a] Equilibrium structure. [b] Approximate transition state structure. [c] All bond distances are in angstroms and all angles are in degrees.

TABLE 10: Calculated Energies (in hartrees) of Molecules Involved in Reactions with Aromatics in This Study[a]

molecule	E_e^{0} [b]	E^{298} [c]
OH	−75.7268	−75.7153
O_2	−150.3165	−150.3093
H_2O	−76.4190	−76.3943
HONO	−205.6981	−205.6736
NO_2	−205.0700	−205.0573
NO	−129.8879	−129.8803

[a] Structures optimized by using PM3 and energies determined by using Becke3LYP/6-31g**. [b] Electronic energy at 0 K. [c] Corrected energies at 298 K, which includes zero-point energies and thermal corrections determined by using PM3 normal mode vibrations.

TABLE 11: Calculated Energies (in hartrees) of the Products Formed by the Reactions of NO_2 with the Toluene−OH Adduct

molecule	E_e^{0}	E^{298}
3-nitrotoluene	−476.0749	−475.9356
2-cresol	−346.7967	−346.6581
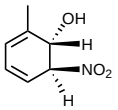	−552.4537	−552.2865
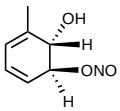	−552.4548	−552.2894
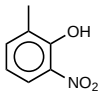	−551.2802	−551.1439
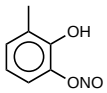	−551.2802	−551.1342

additional computational work is required to fully elucidate the pathways of aromatic−OH reactions with NO_2.

3.3. Aromatic Peroxy Radical. Under atmospheric conditions, oxygen is expected to rapidly add to the aromatic−OH adduct, forming a peroxy radical (reaction 2b in the generalized mechanism).[26] Semiempirical geometry optimizations and *ab initio* calculations were performed on all of the resulting peroxy radicals for each of the five aromatics considered. Transition state analyses indicate that the transition state energies are governed by consideration of the type of carbon atom being bonded to (secondary versus tertiary) and the steric nature of the site of attachment. The energies of the approximated transition states for the reactions of aromatic−OH adducts with O_2 are available in Table 12. From this table, it can be seen that the addition of O_2 to a site adjacent to the OH group (such as O_2 addition to the 3-position with OH at the 2-position for *p*-xylene) results in a transition state energy that is roughly 10 kcal/mol higher than the parent aromatic−OH adduct + O_2 energy. Additions of O_2 to a tertiary carbon give a transition state energy that is roughly 7 kcal/mol higher than the parent aromatic−OH + O_2 energy. Additions to a secondary carbon site not adjacent to the OH radical addition site give a transition state energy that is roughly 5 kcal/mol higher than the parent aromatic−OH + O_2 energy. These barrier heights are consistent with the low rate constants observed by Knispel *et al.*[26] Table 13 contains the geometrical information for the structures of a representative set of the peroxy radicals. Energies for the most stable peroxy radical structures appear in Table 8. Examination of the relative energies of each of the peroxy radicals for a given aromatic reveals that the energies of the intermediate peroxy radicals are all similar. Given this fact, all structural isomers of the aromatic peroxy radicals are equally likely to form.

3.4. Fate of the Peroxy Radical: Cyclization versus NO Reaction. Alkylperoxy radicals present in polluted atmospheres generally react with NO to form alkoxy radicals.[2,28] Aromatic peroxy radicals, in contrast, were postulated to cyclize to form bicyclic radicals to rationalize the observed formation of α-dicarbonyls from the aromatic hydrocarbon reactions.[29] To test this hypothesis, we examined the ΔH_{rxn} for reactions 4 and 5 in the generalized mechanism for aromatic−OH reaction.

Calculations were performed for reaction 4 on all possible bicyclic radicals, regardless of whether or not they originated from the lowest energy aromatic−OH adduct, with the exception of those radicals containing a four-membered oxygen ring. The ring strain energies associated with the formation of such radicals were assumed to be much higher than those of the corresponding five- and six-membered rings. Structural information for selected bicyclic peroxy radicals resulting from the aromatic−OH reaction appear in Table 14. Energies of the most stable bicyclic peroxy radical intermediates appear in Table 8 under the heading of "O_2 bridge formation". In all of the cases studied, the allylically stabilized five-membered bicyclic radicals

TABLE 12: Approximate Transition State Energies for the Reactions of Aromatic−OH Adducts with O_2

aromatic	addition site[a]	ortho groups[b]	E_e^0(TS) (au)	E^{298}(TS) (au)	r(C−O)[c] (Å)	E^{298}(reactants) (au)	barrier height (kcal/mol)
p-xylene	C_s	Me, OH	−536.9635	−536.7780	1.90	−536.7904	7.8
	C_t	H, OH	−536.9673	−536.7818	1.85	−536.7904	5.4
	C_s	H, Me	−536.9669	−536.7814	1.85	−536.7904	5.6
toluene	C_s	H, OH	−497.6406	−497.4857	1.90	−497.4995	8.7
	C_t	H, OH	−497.6454	−497.4905	1.85	−497.4995	5.6
	C_s	H, H	−497.6491	−497.4942	1.80	−497.4995	3.3
m-xylene	C_t	H, OH	−536.9686	−536.7833	1.90	−536.8023	11.9
m-ethyltoluene	C_t(Et)	H, OH	−576.2861	−576.0711	1.80	−576.0779	4.3
	C_t	H, OH	−576.3803	−576.0631	1.85	−576.0779	9.3
	C_s	H, H	−576.2892	−576.0742	1.80	−576.0779	2.3

[a] Represented in terms of the local structure of the aromatic−OH adduct at the addition site, where all tertiary carbons (C_t) are bound to methyl (Me) groups unless indicated. [b] In the two positions ortho to the addition site. [c] Transition state bond distance for the C−O bond that is formed in the addition of O_2. Structures were obtained by using the constrained optimization procedure described in Section 2.

TABLE 13: PM3 Equilibrium Structures for a Representative Selection of the Most Stable Reaction Products of Aromatic−OH Adducts with O_2 (Reaction 2b)[a]

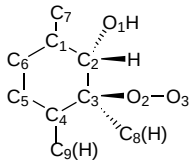

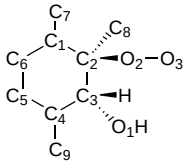

parameter	toluene	*m*-xylene	*p*-xylene	*m*-ethyltoluene	parameter	1,2,4-tmb
$r(C_1,C_2)$	1.510	1.514	1.510	1.513	$r(C_1,C_2)$	1.512
$r(C_2,O_1)$	1.411	1.409	1.410	1.420	$r(C_3,O_1)$	1.409
$r(C_2,C_3)$	1.555	1.563	1.556	1.562	$r(C_2,C_3)$	1.566
$r(C_3,O_2)$	1.478	1.494	1.478	1.496	$r(C_2,O_2)$	1.497
$r(O_2,O_3)$	1.253	1.253	1.255	1.252	$r(O_2,O_3)$	1.252
$r(C_3,C_4)$	1.494	1.504	1.501	1.503	$r(C_3,C_4)$	1.512
$r(C_4,C_5)$	1.345	1.343	1.356	1.345	$r(C_4,C_5)$	1.354
$r(C_5,C_6)$	1.443	1.448	1.440	1.445	$r(C_5,C_6)$	1.440
$r(C_6,C_1)$	1.351	1.349	1.354	1.350	$r(C_6,C_1)$	1.358
$r(C_1,C_7)$	1.482	1.481	1.481	1.482	$r(C_1,C_7)$	1.483
$r(C_3,C_8)$		1.525		1.543	$r(C_2,C_8)$	1.526
$r(C_4,C_9)$			1.482		$r(C_4,C_9)$	1.480
$\angle(C_3,O_2,O_3)$	114	116	114	117	$\angle(C_2,O_2,O_3)$	116
$\angle(C_1,C_2,C_3,O_1)$	125	124	125	121	$\angle(C_2,C_3,C_4,O_1)$	125
$\angle(C_2,C_3,C_4,O_2)$	118	117	117	122	$\angle(C_1,C_2,C_3,O_2)$	118

[a] All bond distances are in angstroms and angles are in degrees.

TABLE 14: PM3 Equilibrium Structures for a Representative Selection of the Most Stable Reaction Products in the Formation of Bicyclic Endoperoxy Radicals from Peroxy Radical Intermediates (Reaction 2b)[a]

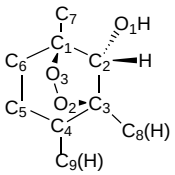

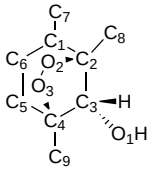

parameter	toluene	*m*-xylene	*p*-xylene	*m*-ethyltoluene	parameter	1,2,4-tmb
$r(C_1,C_2)$	1.577	1.572	1.577	1.570	$r(C_1,C_2)$	1.518
$r(C_2,O_1)$	1.388	1.389	1.388	1.389	$r(C_3,O_1)$	1.389
$r(C_2,C_3)$	1.565	1.572	1.565	1.572	$r(C_2,C_3)$	1.574
$r(C_3,O_2)$	1.403	1.424	1.402	1.423	$r(C_2,O_2)$	1.424
$r(O_2,O_3)$	1.595	1.580	1.595	1.580	$r(O_2,O_3)$	1.580
$r(C_1,O_3)$	1.422	1.424	1.422	1.423	$r(C_4,O_3)$	1.423
$r(C_3,C_4)$	1.505	1.510	1.511	1.511	$r(C_3,C_4)$	1.570
$r(C_4,C_5)$	1.393	1.393	1.402	1.393	$r(C_4,C_5)$	1.509
$r(C_5,C_6)$	1.393	1.393	1.389	1.393	$r(C_5,C_6)$	1.387
$r(C_6,C_1)$	1.511	1.510	1.510	1.511	$r(C_6,C_1)$	1.404
$r(C_1,C_7)$	1.519	1.519	1.519	1.519	$r(C_1,C_7)$	1.473
$r(C_3,C_8)$		1.519		1.532	$r(C_2,C_8)$	1.521
$r(C_4,C_9)$			1.471		$r(C_4,C_9)$	1.520
$\angle(C_1,C_2,C_3,O_1)$	125	125	114	114	$\angle(C_2,C_3,C_4,O_1)$	114
$\angle(C_2,C_3,C_4,O_2)$	114	112	114	112	$\angle(C_1,C_2,C_3,O_2)$	115
$\angle(C_6,C_1,C_2,O_3)$	116	115	115	116	$\angle(C_3,C_4,C_5,O_3)$	112

[a] All bond distances are in angstroms and angles are in degrees.

TABLE 15: Approximate Transition States for the Addition Reactions of Bicyclic Endoperoxy Radical with O_2

aromatic	addition site[a]	ortho groups[b]	E_e^0(TS)	E^{298}(TS)	r(C−O)[c]	E^{298}(reactants)	barrier height (kcal/mol)
toluene	C_s	Me, H	−647.9641	−647.7973	1.9	−647.8262	18.2
	C_s	CO, H	−647.9643	−647.7975	1.9	−647.8262	18.0
p-xylene	C_t	CO, H	−687.3104	−687.1114	1.9	−687.1201	5.5

[a] Represented in terms of the local structure of the bicyclic endoperoxy radical at the addition site. [b] In the two positions ortho to the addition site. Me represents a methyl group bond to a tertiary carbon, whereas CO represents an attachment site for the O_2 bridge. [c] Transition state bond distance for the C−O bond that is formed in the addition of O_2.

TABLE 16: Calculated Energies (in hartrees) for the Products of the Reaction of NO with a Representative Selection of the Most Stable Peroxy Intermediates and for the Products of the Reaction of O_2 with a Representative Selection of the Most Stable Bicyclic Intermediates

molecule	OH site	O• site	E_e^0	E^{298}	OH site	O_2 bridge sites	O_2 addition site	E_e^0	E^{298}
toluene	2	3	−422.4566	−422.3062	2	3, 1	4	−648.0151	−647.8483
m-xylene	2	3	−461.8238	−461.6413	2	3, 1	4	−687.3402	−667.1399
p-xylene	2	3	−461.7941	−461.6131	2	3, 1	6	−687.3344	−687.1354
1,2,4-trimethylbenzene	5	4	−501.1425	−500.9301	5	4, 6	3	−726.6533	−726.4208
m-ethyltoluene	6	5	−501.1191	−500.9067	6	5, 1	2	−726.6518	−726.4236

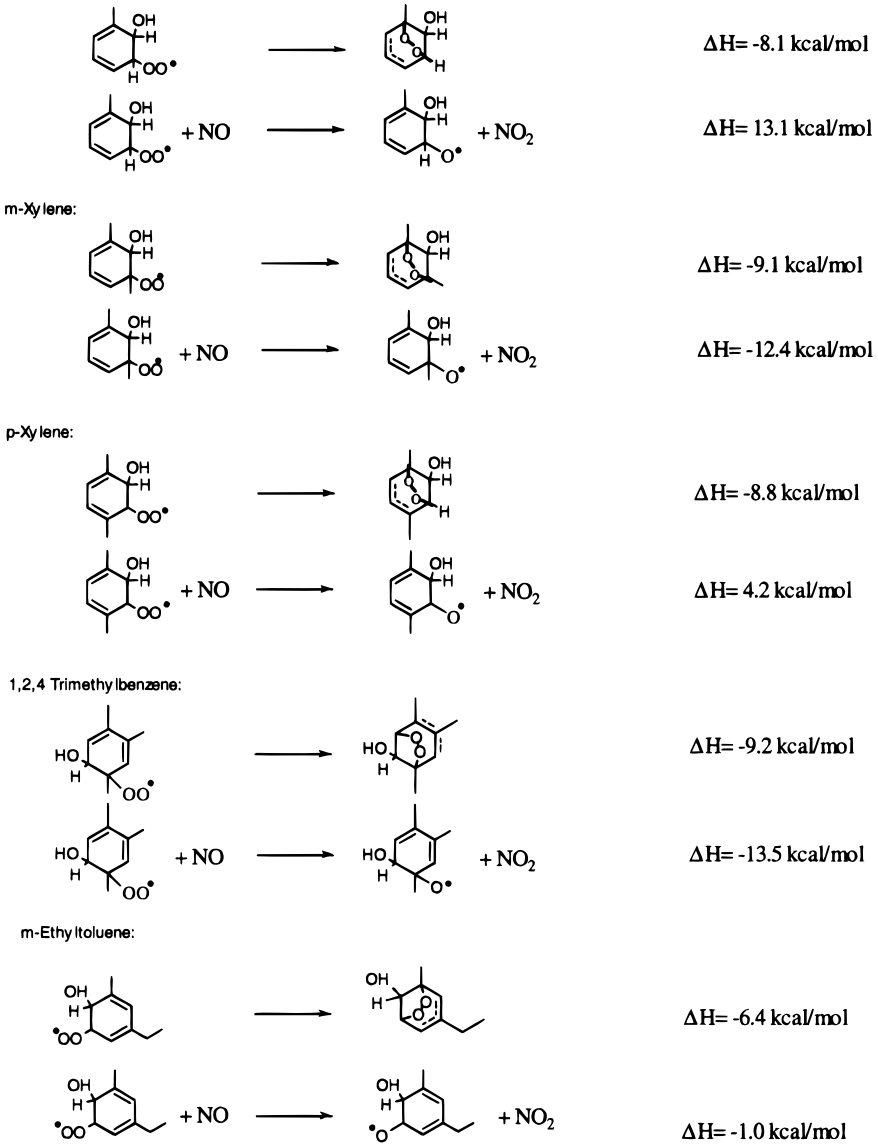

Figure 7. ΔH_{rxn} values for reactions 4 and 5 for different aromatic systems.

are the lowest energy bicyclic radicals formed. In fact, all other nonallylically stabilized bicyclic radicals are about 20 kcal higher in energy than the lowest energy allylically stabilized bicyclic radical and are approximately 10 kcal/mol higher in energy than the corresponding peroxy radicals from which they are formed. Thus, the reactions forming the allylically stabilized bicyclics are the only exothermic reactions determined in this step of the mechanism. The barrier heights for bicyclic ring closure seem to be governed by the attachment sites of the O_2 bridge. Representative transition state energies for the bicyclic radical intermediates appear in Table 15. A transition state that results in the attachment of an O_2 bridge to two tertiary carbons

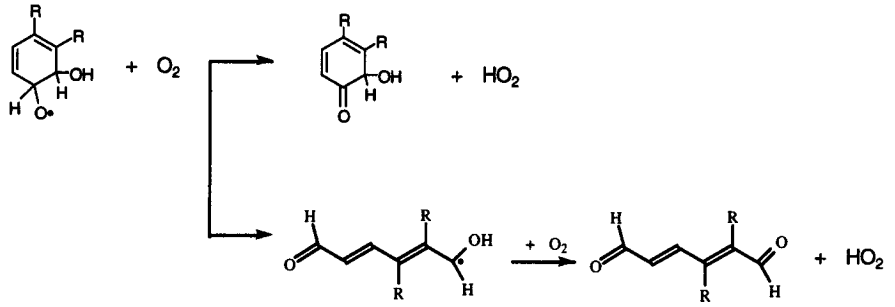

Figure 8. Subsequent reaction of oxy radicals formed from reaction 5 of the generalized mechanism.

TABLE 17: Approximate Transition States for the Formation of the Bicyclic Endoperoxy Radical

aromatic	peroxy site[a]	endoperoxy attachment site[b]	E_e^0(TS) (au)	E^{298}(TS) (au)	r(C−O)[c] (Å)	E^{298}(peroxy) (au)	barrier height (kcal/mol)
m-xylene	C_t	C_t	−536.9672	−536.7800	2.20	−536.7986	11.7
toluene	C_s	C_t	−497.6318	−497.4764	2.10	−497.5040	17.3
	C_t	C_s	−497.6396	0497.4842	2.05	−497.5040	12.4
p-xylene	C_t	C_s	−536.9625	−536.7775	2.05	−536.7968	12.1

[a] Represented in terms of the type of carbon that is bound to an oxygen at the original site of O_2 addition for the peroxy radical and [b]at the bond that is created when the O_2 is formed. [c] Transition state bond distance for the bond that is created when the O_2 bridge is formed.

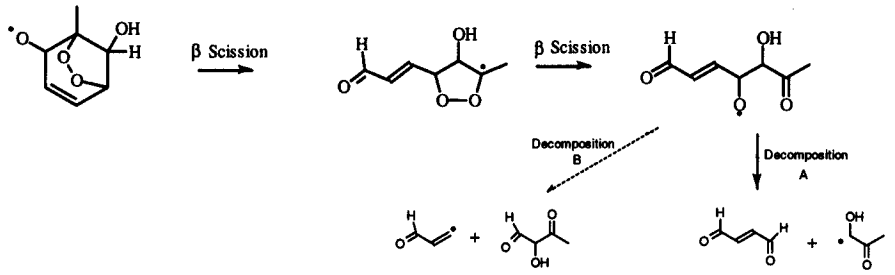

Figure 9. β-scission of a bicyclic oxy radical of toluene to give ring fragmentation products. Decomposition path A is the favored path for fragmentation of the acyclic radical.

results in a lower energy transition state than that that results in the attachment to one tertiary and one secondary carbon. The energy of the transition state that results in an O_2 bridge between two tertiary carbons is approximately 10 kcal/mol higher than that of the parent peroxy radical. A transition state that results in O_2 attachment to a secondary carbon, with O_2 originating from a tertiary site, results in a transition state energy that is approximately 12 kcal/mol higher than that of the parent peroxy radical. A transition state that results in O_2 attachment to a tertiary carbon, with O_2 originating from a secondary carbon site, results in a transition state energy that is approximately 17 kcal higher than that of the parent peroxy radical.

Energy data for a representative selection of aromatic oxy radicals formed in the reaction of NO with the aromatic peroxy radicals appear in Table 16. Representative aromatic peroxy radicals, bicyclic radicals, and aromatic oxy radicals, along with the ΔH_{rxn} values for reactions 4 and 5, are presented in Figure 7. Not all of the lowest energy aromatic peroxy radicals (which appear in the reaction coordinate diagrams) appear in Figure 7. The peroxy radicals chosen for Figure 7 are representative cases chosen to give the reader an indication that the two pathways for peroxy radical reaction are both possible and that reaction 5 cannot be unambiguously excluded from a generalized reaction mechanism. Inclusion of reaction 5 results in the formation of oxy radicals. These radicals can go on to react according to the scheme in Figure 8 to yield ring-retained hydroxy carbonyl compounds or decompose by C−C bond scission to ultimately form a di-unsaturated dicarbonyl. These carbonyl compounds can serve to account for part of the carbon unaccounted for in laboratory studies of aromatic−OH systems.

3.5. Bicyclic Peroxy Radicals. After bicyclic radical formation, oxygen quickly adds to the radical, forming a bicyclic peroxy radical. Transition state energies for a representative selection of bicyclic peroxy radicals appear in Table 17. Energy calculations were performed on each of the resulting possible bicyclic peroxy radicals. Note that O_2 addition to rings that result in bicyclic peroxy structures with two radical sites is unlikely to form and thus was not subjected to single-point calculations. The energies determined for the bicyclic peroxy radicals are all similar in magnitude; thus, all bicyclic peroxy structures resulting from the lowest energy bicyclic radicals must be considered in an overall mechanism. Given the steric hindrance problems associated with another cyclization, the bicyclic peroxy radical reacts with NO to form a bicyclic oxy radical and NO_2.

3.6. Ring Fragmentation Products. The only path for the resulting bicyclic oxy radicals is fragmentation via favorable β-scission reactions. These fragmentation reactions yield an acyclic radical and eventually dicarbonyl products (see Tables 1−3). Shown in Figure 9 is an example of the β-scission process for a bicyclic oxy radical formed in the photooxidation of toluene. The key issue is the method of fragmentation of the resulting acyclic radical. Calculations of the ΔH_{rxn} for the decomposition of the acyclic radical were conducted by using the NIST Structures and Properties estimation program.[25] This program is based on the group additivity theory of Benson.[30] On the basis of the calculations, each acyclic radical fragments at the bond between the carbon attached to the oxygen atom and the saturated carbon center rather than the unsaturated carbon center. This point is clearly shown in Figure 9. Decomposition path A, illustrating fragmentation between the carbon with the oxygen atom attached to it and the unsaturated carbon center, is the favored path on the basis of group additivity calculations. Decomposition path B is the unlikely method of

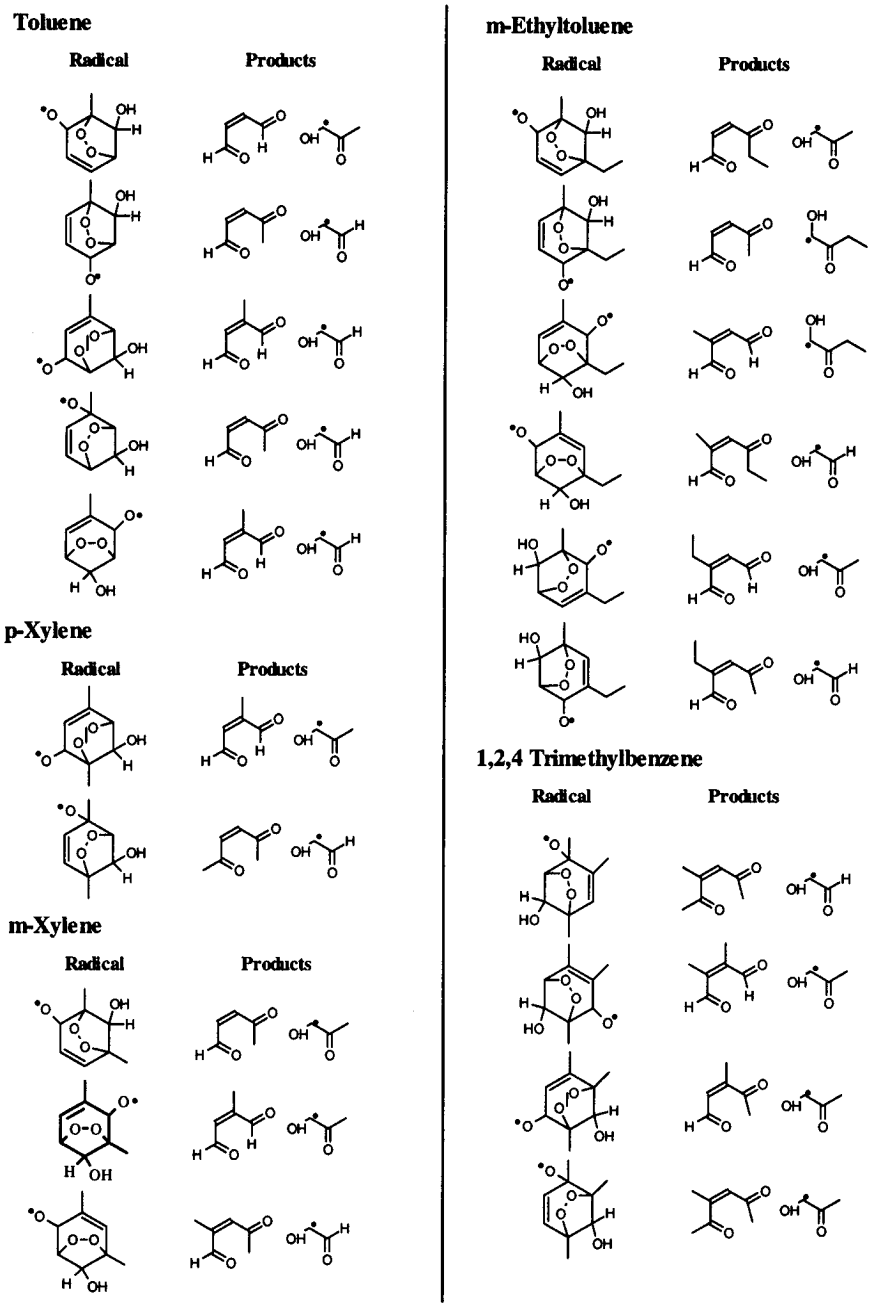

Figure 10. Fragmentation products formed from the bicyclic oxy radicals.

fragmentation on the basis of group additivity considerations. Shown in Figure 10 are the bicyclic oxy radicals and the products that are predicted to form following the β-scission process analogous to that depicted in Figure 9. It is well-known that α-hydroxy carbonyls subsequently react with O_2 to form HO_2 and the corresponding dicarbonyl product.[29] Note from Tables 1−3 that a number of the ring fragmentation products theoretically predicted for toluene, *m*-xylene, and *p*-xylene have been identified experimentally.

4. Conclusion

We have elucidated the intermediates in five atmospheric aromatic−OH photooxidation systems by using theoretically based calculations. In general, we find that the predicted site of initial OH attack is ortho to a substituent group attached to the ring. In addition, we have investigated the NO_2 reaction with the aromatic−OH adduct and have shown that this reaction proceeds via four pathways, forming the nitroaromatic (reaction 3a), hydroxynitroaromatic (reaction 3b), hydroxyaromatic nitrite (reaction 3c), and phenolic compound (reaction 3d). Reaction 3e is not energetically favored and thus is excluded from a general aromatic−OH mechanism. All peroxy radicals formed from the reaction of the aromatic adduct with O_2 have approximately the same energy. Therefore, it is difficult to exclude a particular structure. However, it is clear that if the original aromatic−OH adduct is not favored, then the resulting peroxy radicals will not be formed.

The allylically stabilized five-membered-ring bicyclic radicals are, in all cases, approximately 20 kcal/mol more stable than any other bicyclic radical, including those with six-membered rings. Thus, these bicyclic radicals should be included in overall aromatic reaction mechanisms. The aromatic peroxy radical reaction with NO (reaction 5) is determined to be a plausible reaction to include in aromatic−OH reaction mechanisms. Subsequent reaction of the oxy radicals formed in reaction 5 can lead to ring-retaining hydroxy carbonyl compounds. These

additional ring-retaining compounds can account for part of the remaining carbon unaccounted for in laboratory studies of aromatics. When compared to available product data, the theoretical results for the intermediates formed and the subsequent reactions for toluene, *m*-xylene, and *p*-xylene are found to be consistent with experimental results. The theoretical technique has been applied to two important, yet relatively unstudied aromatics, 1,2,4-trimethylbenzene and *m*-ethyltoluene, to predict their reaction intermediates and stable products.

Acknowledgment. This work was supported by the U.S. Environmental Protection Agency Center for Airborne Organics (R-819714-01-0), National Science Foundation Grant ATM-9307603, the Coordinating Research Council (A-5-1), and the Chevron Corporation. The authors thank J. K. Perry and T. Jungkamp for helpful discussions.

References and Notes

(1) National Research Council; *Rethinking the Ozone Problem in Urban and Regional Air Pollution*; National Academy Press: Washington, D.C., 1991.

(2) Atkinson, R. *J. Phys. Chem. Ref. Data, Monograph 1*, **1989**, 1.

(3) Atkinson, R. *J. Phys. Chem. Ref. Data, Monograph 2*, **1994**, 1.

(4) Atkinson, R. *Atmos. Environ.* **1990**, *24A*, 1.

(5) Bandow, H.; Washida, N. *Bull. Chem. Soc. Jpn.* **1985**, *58*, 2549.

(6) Tuazon, E.; MacLeod, H.; Atkinson, R.; Carter, W. *Environ. Sci. Technol.* **1986**, *20*, 383.

(7) Dumdei, B.; Kenny, D.; Shepson, P.; Kleindienst, T.; Nero, C.; Cupitt, L.; Claxton, L. *Environ. Sci. Technol.* **1988**, *22*, 1493.

(8) Bandow, H.; Washida, N.; Akimoto, H. *Bull. Chem. Soc. Jpn.* **1985**, *58*, 2531.

(9) Shepson, P.; Edney, E.; Corse, E. *J. Phys. Chem.* **1984**, *88*, 4122.

(10) Atkinson, R.; Aschmann, S.; Arey, J.; Carter, W. *Int. J. Chem. Kinet.* **1989**, *21*, 801.

(11) Bandow, H.; Washida, N. *Bull. Chem. Soc. Jpn.* **1985**, *58*, 2541.

(12) Gery, M.; Fox, D.; Kamens, R.; Stockburger, L. *Environ. Sci. Technol.* **1987**, *21*, 339.

(13) Atkinson, R.; Aschmann, S.; Arey, J. *Int. J. Chem. Kinet.* **1991**, *23*, 77.

(14) Parr, R. G.; Yang, W. *Density Functional Theory of Atoms and Molecules*; Oxford University Press: New York, 1989; Chapter 3.

(15) Becke, A. D. *Phys. Rev. A* **1988**, *38*, 3098.

(16) Becke, A. D. *ACS Symp. Ser.* **1989**, *394*, 165.

(17) Lee, H.; Lee, C.; Parr, R. G. *Phys. Rev. A* **1991**, *44*, 768.

(18) Frisch, M. J.; Trucks, G. W.; Schlegel, H. B.; Gill, P. M. W.; Johnson, B. G.; Wong, M. W.; Foresman, J. B.; Robb, M. A.; Head-Gordon, M.; Replogle, E. S.; Gompert, R.; Andres, I. L.; Raghavachari, K.; Binkley, J. S.; Gonzalez, C.; Martin, R. L.; Fox, D. J.; Defrees, D. J.; Baker, J.; Stewart, J. J. P.; Pople, J. A. *Gaussian 92/DFT, Revision F.4*; Gaussian, Inc.: Pittsburg, PA, 1993.

(19) Stewart, J. J. P. *J. Comput. Chem.* **1989**, *10*, 209.

(20) Allinger, N. L. *J. Am. Chem. Soc.* **1977**, *99*, 8127.

(21) Plummer, B. F.; Steffen, W. C.; Herndon, W. C. *Struct. Chem.* **1993**, *4*, 279.

(22) Coolidge, M. B.; Marlin, J. E.; Stewart, J. J. P. *J. Comput. Chem.* **1991**, *12*, 948.

(23) Ringnalda, M. N.; Langlois, J. M.; Greeley, B. H.; Murphy, R. B.; Russo, T. V.; Cortis, C.; Muller, R. P.; Martin, B.; Donnelly, R. E., Jr.; Mainz, D. T.; Wright, J. R.; Pollard, W. T.; Cao, Y.; Won, Y.; Miller, G. H.; Goddard, W. A., III; Friesner, R. A. *PSGVB version 2.1*; Schrodinger, Inc.: Corvallis, OR, 1995.

(24) *Hyperchem Release 4.0*; Autodesk, Inc.: Waterloo, Ontario, Canada, 1994.

(25) Stein, S. E.; Rukkers, J. M.; Brown, R. L. *NIST Standard Reference Database 25: NIST Structures and Properties Database and Estimation Program*; NIST: Gaithersburg, MD, 1991.

(26) Knispel, R.; Koch, R.; Siese, M.; Zetzsch, C. *Ber. Bunsenges. Phys. Chem.* **1990**, *94*, 1375.

(27) Atkinson, R.; Aschmann, S. M. *Int. J. Chem. Kinet.* **1994**, *26*, 929.

(28) Wallington, T. J.; Dagaut, P.; Kurylo, M. J. *Chem. Rev.* **1992**, *92*, 667.

(29) Atkinson, R.; Lloyd, A. *J. Phys. Chem. Ref. Data* **1984**, *13*, 315.

(30) Benson, S. W. *Thermochemical Kinetics*, 2nd ed.; John Wiley & Sons: New York, 1976.

JP952935L